

The 2nd Technical Note of AMON-ES (TN2-AE)

SK2-09: Follow-up of feasibility study to observe
ionospheric disturbances by airglow monitoring network
(AMON-net)

*Department of Space Physics
Institute of Experimental Physics, Slovak Academy of Sciences
Košice, Slovakia*

ESA Contract No. 4000125330/18/NL/SC,
Plan for European Cooperating States (PECS) in Slovakia
January 2020

Contents

Revision History	1
1 Introduction	2
1.1 Purpose	2
1.2 Document Overview	2
1.3 Intended Audience	2
1.4 Acronyms and Abbreviations	3
1.5 References	4
2 Recapitulation of 1st Technical Note of AMON-ES (TN1-AE)	5
3 Airglow MONitor - Extended Station (AMON-ES) operation	6
3.1 Airglow monitoring system	6
3.2 Ionosphere monitoring system	12
3.3 Weather monitoring system	21
4 Conclusions and Next steps	23

Revision History

Revision	Date	Author(s)	Description
1.0	30. 01. 2020	S. Mackovjak	Submitted version for AR and ORR

Chapter 1

Introduction

1.1 Purpose

The 2nd Technical Note of AMON-ES (TN2-AE) reports the details about the operation of AMON-ES that is a substantial part of the R&D activity "Follow-up of feasibility study to observe ionospheric disturbances by airglow monitoring network (AMON-net)" (SK2-09). The TN2-AE provides description of the 2nd phase of AMON-ES performance, and the results of the measurements that were realized according Technical Note of System Requirements Specification (TN-SRS) and Manufacturing, Assembly, Integration and Test Plan for the AMON-ES (MAITP-AE). This is the continuation of the activity described in TN1-AE.

1.2 Document Overview

The TN2-AE document consists of four major chapters. Introduction (Chapter 1) provides basic information about the document. The recapitulation of the main outcomes from the TN1-AE is provided in Chapter 2. The AMON-ES operation during the 2nd phase is presented in Chapter 3. This chapter also contains the comparison of the AMON-ES results with AMON instrument and the consequences for the construction of Airglow MONitor-network (AMON-net). The conclusions and the next steps are provided in Chapter 4.

1.3 Intended Audience

The AMON-net system is developed by Department of Space Physics (DSP), Institute of Experimental Physics (IEP), Slovak Academy of Sciences (SAS) within the European Space Agency (ESA) / Plan for European Cooperating States (PECS) in Slovakia. The AMON-ES is the substantial part of AMON-net development process. The 2nd Technical Note of AMON-ES (TN2-AE) is a deliverable to ESA team, that provides support to Cooperating States, for the review within the 3rd Milestone - Acceptance Review & Operational Readiness Review

(AR-ORR). It will be essentially used by DSP staff to continue in R&D activity SK2-09.

1.4 Acronyms and Abbreviations

AAC	AMON All-sky Camera
AMON	Airglow MONitor
AMON-ES	Airglow MONitor - Extended Station
AMON-net	Airglow MONitor - network
AOK	Astronomical Observatory on Kolonica Saddle
AR-ORR	Acceptance Review & Operational Readiness Review
AGW	Atmospheric Gravity Waves
DSP	Department of Space Physics
ESA	European Space Agency
IEP	Institute of Experimental Physics
MAITP-AE	Manufacturing, Assembly, Integration and Test Plan for the AMON-ES
PECS	Plan for European Cooperating States
R&D	Research & Development
SAS	Slovak Academy of Sciences
SK1-05	"Feasibility study to observe ionospheric disturbances by one pixel UV detector"
SK2-09	"Follow-up of feasibility study to observe ionospheric disturbances by airglow monitoring network (AMON-net)"
TN-SRS	Technical Note of System Requirements Specification
TN1-AE	1st Technical Note of AMON-ES
TN2-AE	2nd Technical Note of AMON-ES
TN-TS	Technical Note of Theoretical Study
WP2	Work Package 2
WP5	Work Package 5

1.5 References

- [1] T.G Slanger, P.C Cosby, and D.L Huestis. Co-variation of nightglow emission from the o₂(a3) and o₂(c1) states and the oxygen green line, observed with the keck i/ii telescopes. *Journal of Atmospheric and Solar-Terrestrial Physics*, 66(6):617 – 622, 2004. Dynamics and Chemistry of the MLT Region - PSMOS 2002 International Symposium.
- [2] N. P. Perevalova, A. S. Polyakova, and A. V. Zalizovski. Diurnal variations of the total electron content under quiet helio-geomagnetic conditions. *Journal of Atmospheric and Solar-Terrestrial Physics*, 72(13):997–1007, Aug 2010.
- [3] J.S. Haase, T. Dautermann, M.J. Taylor, N. Chapagain, E. Calais, and D. Pautet. Propagation of plasma bubbles observed in brazil from gps and airglow data. *Advances in Space Research*, 47(10):1758 – 1776, 2011. GNSS Remote Sensing-2.

Chapter 2

Recapitulation of TN1-AE

The main goal of construction of AMON-ES was to obtain wider understanding of airglow variation that is observed by one pixel instrument - Airglow MONitor (AMON) and to get clear recognition which variation is caused by airglow dynamics and which is caused by troposphere and astronomical background effects. It was also built to allow comparison of airglow measurements with the ionospheric measurements by using GNSS signal.

In the 1st phase of Work Package 2 (WP2), the AMON-ES has been successfully established at the Astronomical Observatory on Kolonica Saddle (AOK). The mechanical construction, electronic and internet network infrastructure were prepared in conditions that exceed the original requirements (Figure 2.1). The main instruments - AMON All-sky Camera (AAC) and GNSS receiver have been successfully tested, installed and have been operated each cloudless dark night at Astronomical Observatory on Kolonica Saddle (AOK) since May 2019. The data from the initial operation were processed and presented promising results. Whole this process were according to the MAITP-AE. For more details refer to TN1-AE. In what follows we describe in detail the 2nd phase of WP2 and also the results of the Work Package 5 (WP5).



Figure 2.1: The AMON-ES box during installation of the infrastructure.

Chapter 3

AMON-ES operation

3.1 Airglow monitoring system

The main instrument for airglow monitoring within AMON-ES is AMON All-sky Camera (AAC). It is a Moravian Instruments G2-4000 camera with resolution 2056×2062 pixels. It is equipped with Sigma fish-eye lens (focal length - 4.5 mm, angle of view - 180 degrees, aperture - f/2.8), and also with narrow-band and broad-band filters. The characteristics of the filters are listed in Table 3.1 and their transmittance is displayed in Figure 3.1. The transmittance of the fish-eye lens and the glass cover of the external box are displayed in Figure 3.2. The total transmittance of the whole optical system (filter * lens * external glass) is presented in Figure 3.3.

Filter	Filter tag	Wavelength range
Baader U (2458292)	U	315–390 nm
Alluxa 560-10	G	554.5–564.5 nm
Alluxa 632-10	R	627.5–637.5 nm
Hebo R700	I	700–900 nm
Alluxa 568-10	N	563.5–573.5 nm

Table 3.1: The AMON All-sky Camera (AAC) filters.

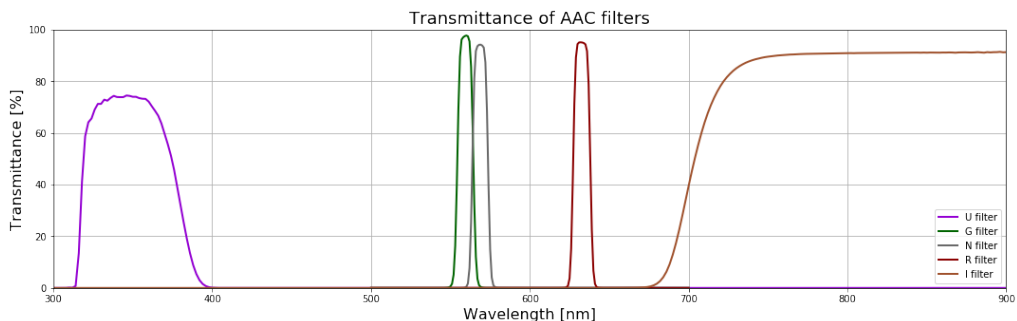


Figure 3.1: The transmittance of the filters of the AMON All-sky Camera (AAC).

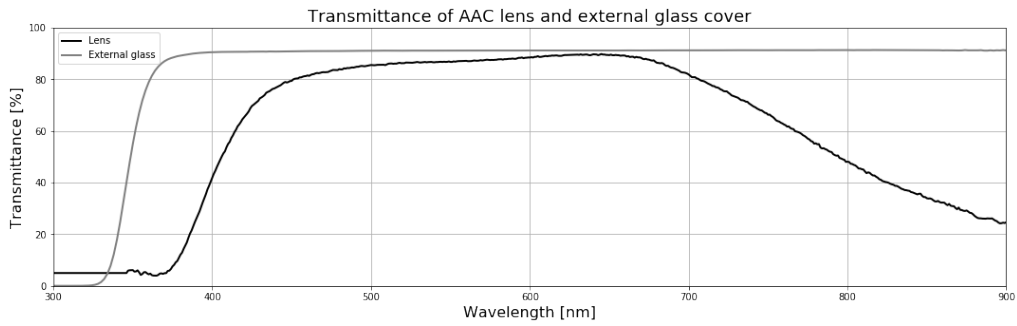


Figure 3.2: The transmittance of the AAC lens and external glass cover.

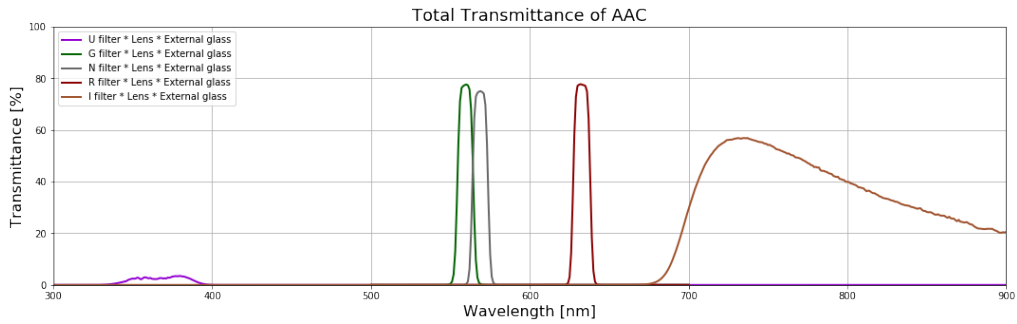


Figure 3.3: The total transmittance of the AAC.

As it is presented in Figure 3.3, the U filter is not compatible with the spectral range of the lens and therefore its total transmittance is very low. This issue might be fixed in the future by extension of UV range of U filter. For now we use 4 filters (G, R, I, N). The contribution of airglow radiation can be distinguished from radiation of astronomical background (stars, Milky Way, and other astronomical sources) by comparison of the images in filters that covers airglow lines (G, R, I) with the filter (N) where no intensive airglow lines are present.

The better overview of the airglow spectrum can be obtained by using Figure 3.4. The spectrum was measured by the main 1m mirror telescope at Astronomical Observatory on Kolonica Saddle (AOK) - the Vihorlat national telescope that is dedicated for observations of variable stars. The byproducts of its observations are spectral measurements of the fields without stars. The main light contribution from this field is produced by airglow. These data will be used in the future analyses.

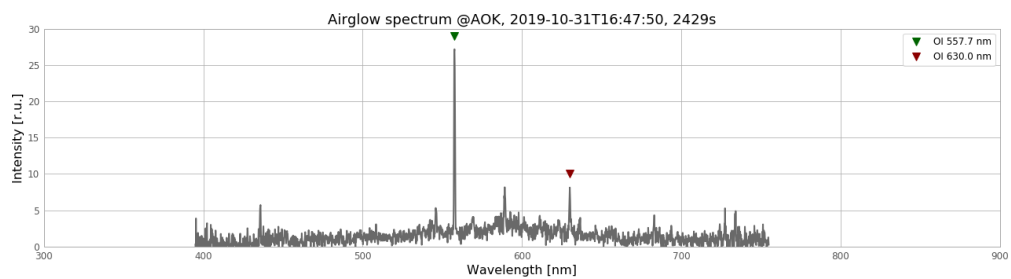


Figure 3.4: The airglow spectrum observed by Vihorlat national telescope on 31 October 2019. The most prominent lines OI 557.7 nm and OI 630.0 nm can be identified easily.

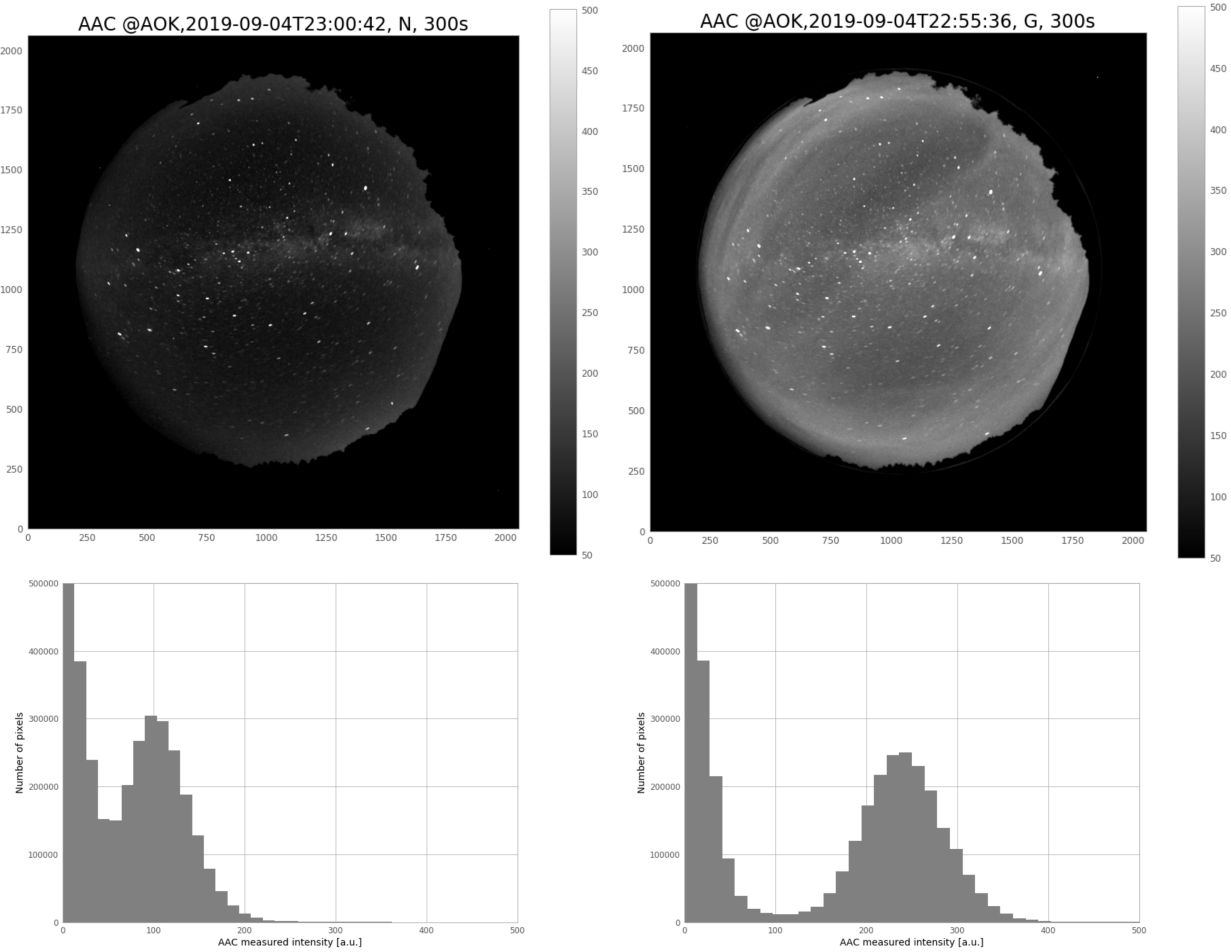


Figure 3.5: The AMON All-sky Camera (AAC) images in N and G filters captured on 4 September 2019. The histograms represent the intensity distribution of the pixels on particular images.

The comparison of the images in G filter (green airglow with most prominent line OI 557.7 nm) and N filter (no airglow lines) is presented in Figure 3.5. The N filter image can be used to remove astronomical background (stars, Milky Way, planets, and etc.) from the airglow images in other filters. The example is displayed in Figure 3.6. The image in N filter was rotated back to eliminate night sky movement around the north celestial pole and then it was subtracted from the image in G filter. Such a cleaned image present the airglow structures and their topology. As it was mentioned above, the G filter is very narrow, so we can observe specific layer of green airglow that is created in the altitude 85–105 km.

The airglow structures are very dynamic. The airglow intensity is changing within minutes and naturally it is different each night. This means that the processes that change the density in the Earth's upper atmosphere are very dynamic (see Technical Note of Theoretical Study (TN-TS) for more details). The example of such processes - the Atmospheric Gravity Waves (AGW) are displayed in Figure 3.7. In this case, the increases and decreases of atomic oxygen densities represented by increases and decreases of green airglow intensities were moved across the AAC field of view. The observation of AGW by AAC was reported already in TN1-AE in I filter. In the second half of the year 2019, we were able to detect them also in G filter. This is important

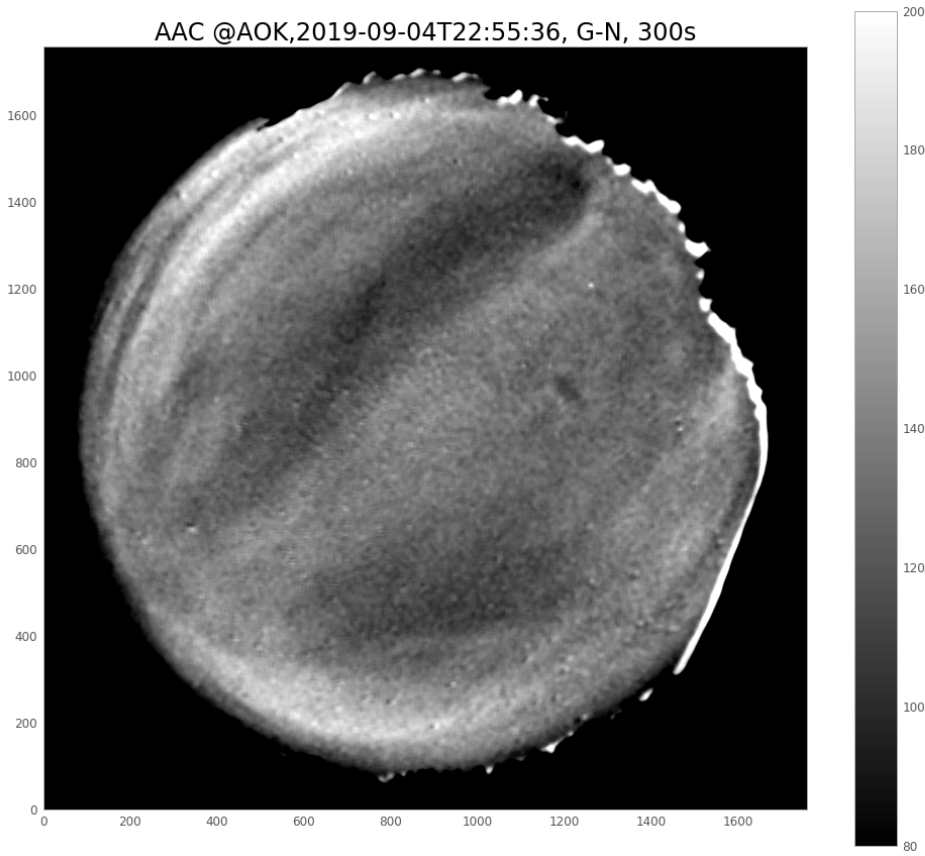


Figure 3.6: The image of green airglow that is a result of the subtraction of N filter image from G filter image presented in Figure 3.5.

for the comparison purposes with the AMON measurements. The dynamic of UV airglow layer observed by AMON is closely connected to dynamic of green airglow observed by AAC G filter. This fact of co-variation is known from literature e.g. [1]. The AMON measurements from the night on 21 - 22 October 2019 are displayed in the Figure 3.8. The AMON measurements are averaged by rolling mean over 300 s. The wave like structures can be clearly recognised in AMON data. The AAC averaged data of the window that roughly correspond to AMON field of view (compare the specified pixels with the position of Polaris star in Figure 3.5) are in good agreement with the trend measured by AMON. This is a clear evidence that AMON can monitor airglow dynamics with very high time resolution. An another example of comparison of the AMON and corresponding AAC measurements is displayed in Figure 3.9. During the moonless night, the AAC images were acquired only in G filter. Thanks to this setup the higher time resolution of AAC was obtained. The airglow variations detected by AMON are in very good agreement with the airglow variations detected by AAC. The combination of both instruments provide overall spatial and temporal representation of the state of the upper Earth's atmosphere. For the purposes of detection of irregularities in the upper atmosphere, the AMON instrument should be sufficient to answer the question if the irregularities are present or not for the particular time. Assuming that the AMON instrument is roughly 10 times cheaper than AAC and data handling and operation is much more straightforward, it should represent a very effective solution for monitoring of airglow variations.

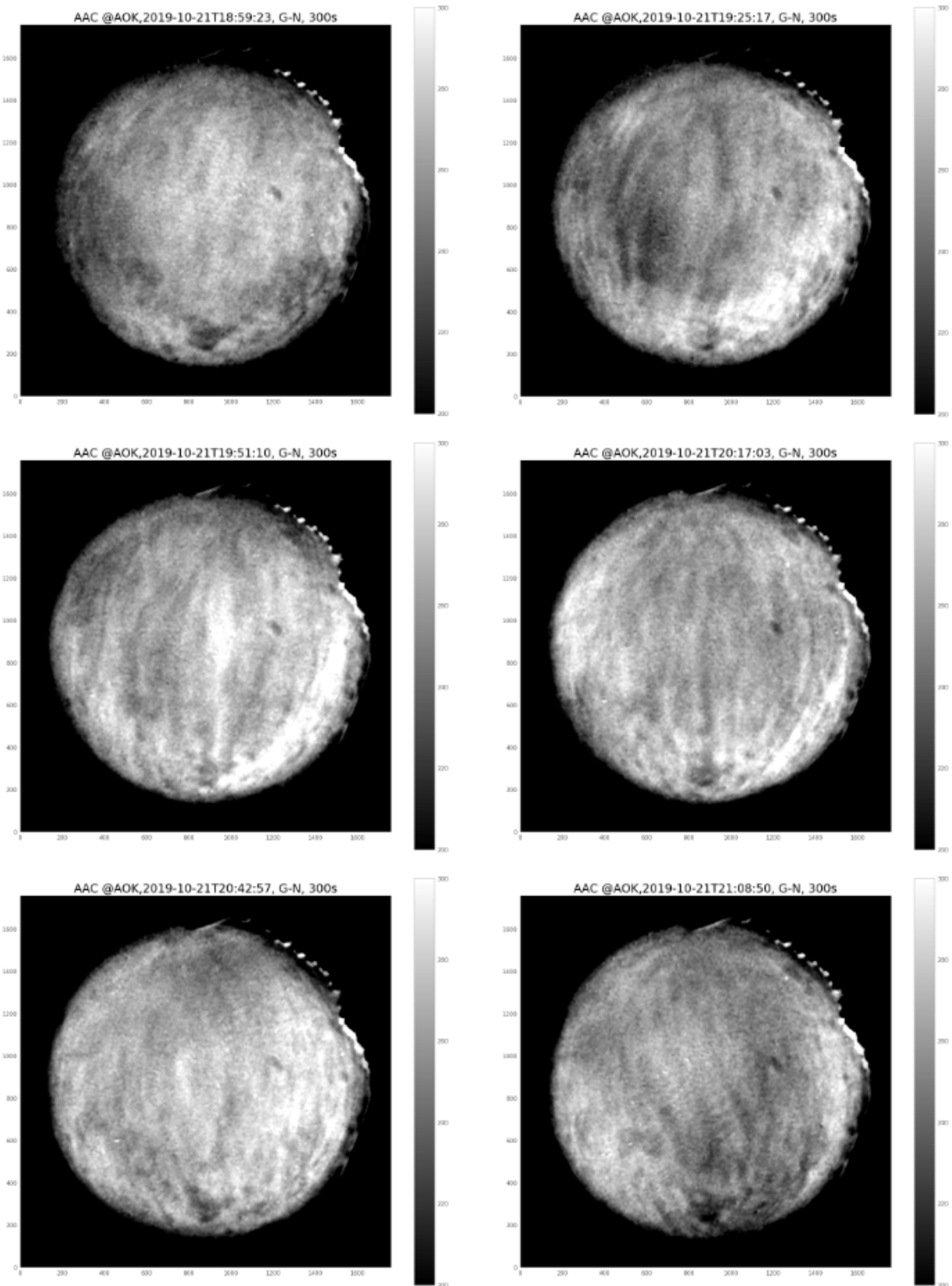


Figure 3.7: The example of Atmospheric Gravity Waves (AGW) penetrating the green airglow during 2 hours on 21 October 2019. The exact time is indicated on the top of each panel. The images were processed by using the same method as Figure 3.6.

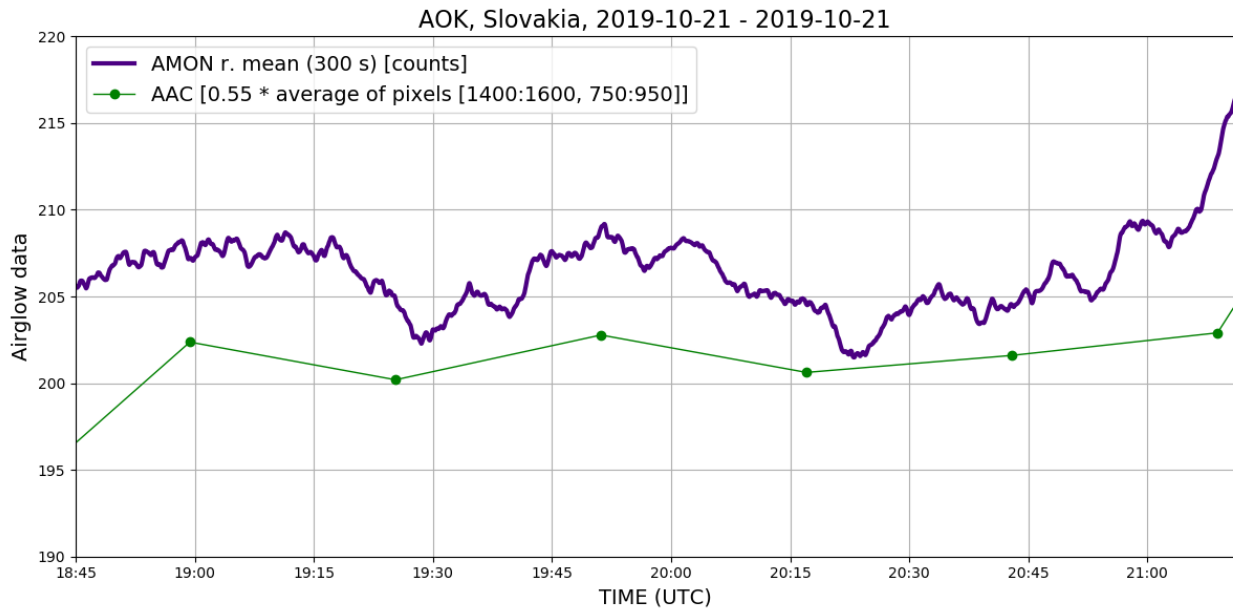


Figure 3.8: The AMON measurements averaged by rolling mean over 300s and the averages of 6 AAC sub-images multiplied by 0.55 to be displayed in the same y-axes interval. The displayed time interval corresponds to the time interval presented in Figure 3.7.

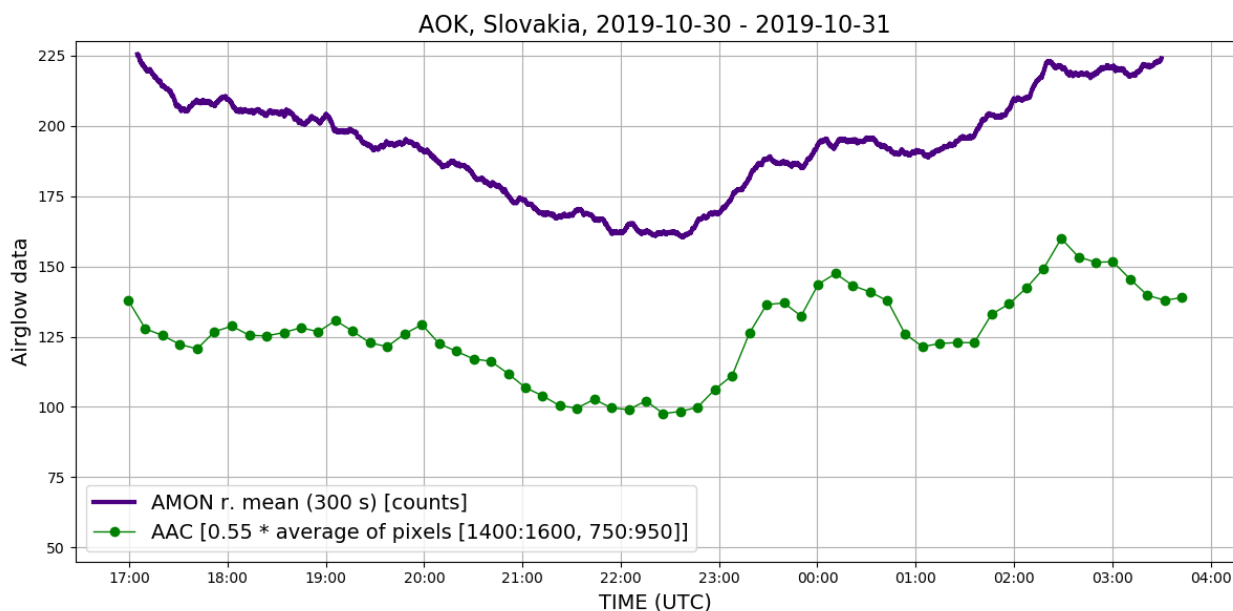


Figure 3.9: The same as in Figure 3.8 but for the observation on 30 October 2019.

3.2 Ionosphere monitoring system

One of the main motivation of construction of AMON-ES was to verify the performance of AMON instrument. As it is presented in Section 3.1 the AMON measurements are consistent with the much advanced instrument for airglow observation - AMON All-sky Camera (AAC). In this section, the measurements of ionospheric parameters by GNSS receiver with antenna are described and possible connections to airglow measurements are presented.

The details about the ionosphere monitoring system are provided in former reports (MAITP-AE and TN1-AE). Basically it consists of GNSS receiver Septentrio PolaRxS with anthena Trimble Zephyr Geodetic Model 2 that were loaned from ESA in spring 2019. The main parameters that are continuously acquired by this instrumentation are: ionospheric scintillation indexes (S_4 (amplitude scintillation), σ_ϕ (phase scintillation), SI (scintillation index)) and total electron content (TEC). These parameters are measured by connection to all available GPS and Galileo satellites for particular time. The examples of these measurements are displayed in Figures 3.10 - 3.13. These figures demonstrate the reliable, continuous, and fully automated operation of the AMON-ES ionosphere monitoring system. They also demonstrate an extensive amount of the data that is growing each minute. To process and analyse such amount of the data, the advanced software tools are required. Their development is beyond the scope of the current activity SK2-09. Even though these data are very valuable especially about detection and prediction of the ionospheric disturbances. For this reason we have proposed a new activity within the Fifth Call for Outline Proposals under the Plan for European Cooperating States (PECS) in Slovakia with the title "Automated tools for ionospheric scintillations prediction based on machine learning techniques (ISP-ML)". The main goal is to demonstrate the proof-of-concept of ISP-ML system.

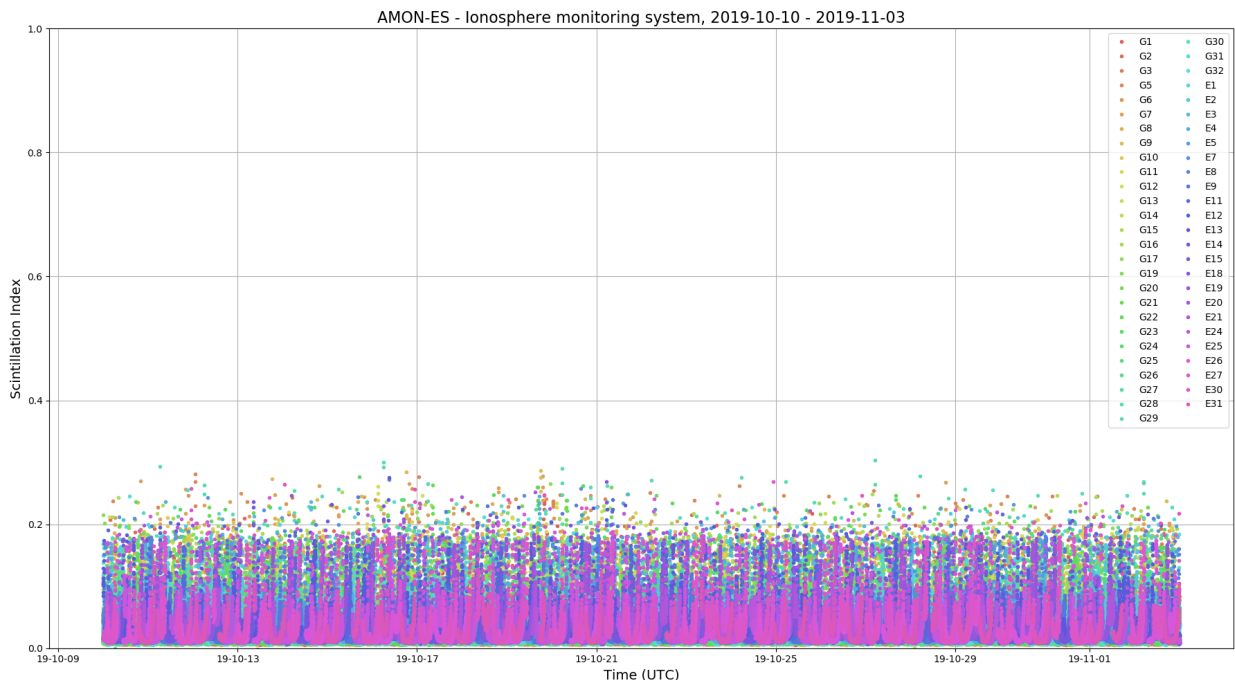


Figure 3.10: The series of SI index measured during 10 October - 3 November 2019. The color coding is according to the specific GPS and Galileo satellites. The time resolution is 1 minute.

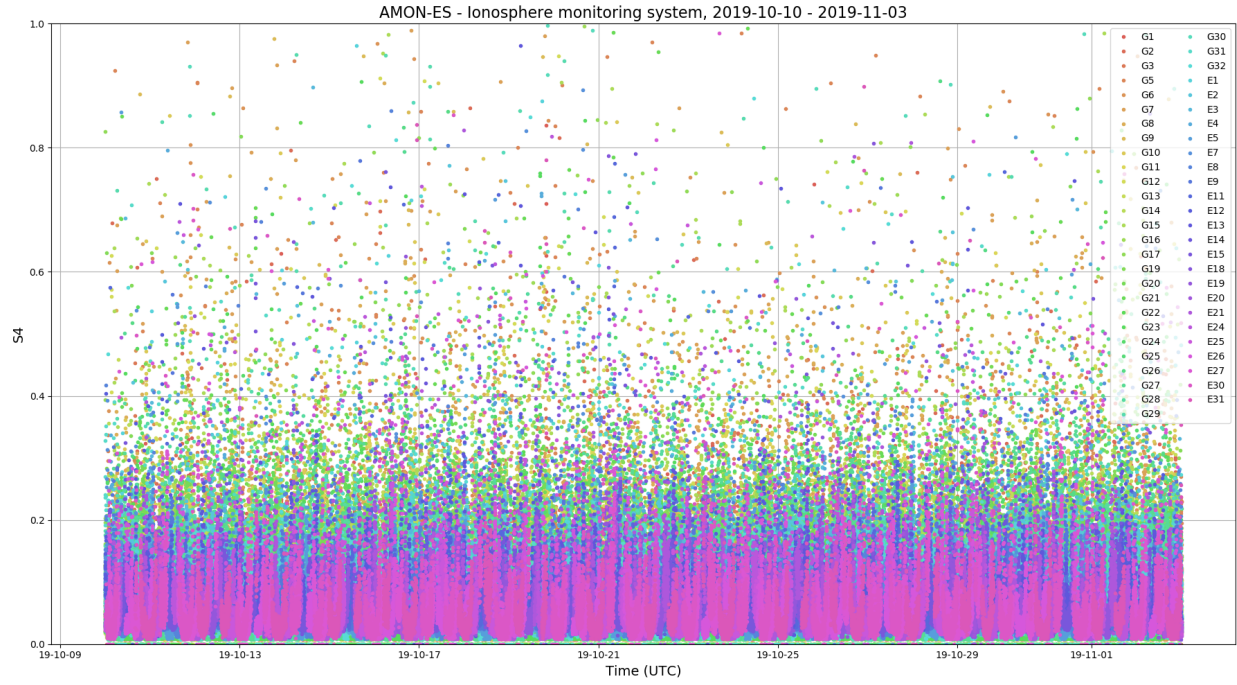


Figure 3.11: The series of S_4 index measured during 10 October - 3 November 2019. The color coding is according to the specific GPS and Galileo satellites. The time resolution is 1 minute.

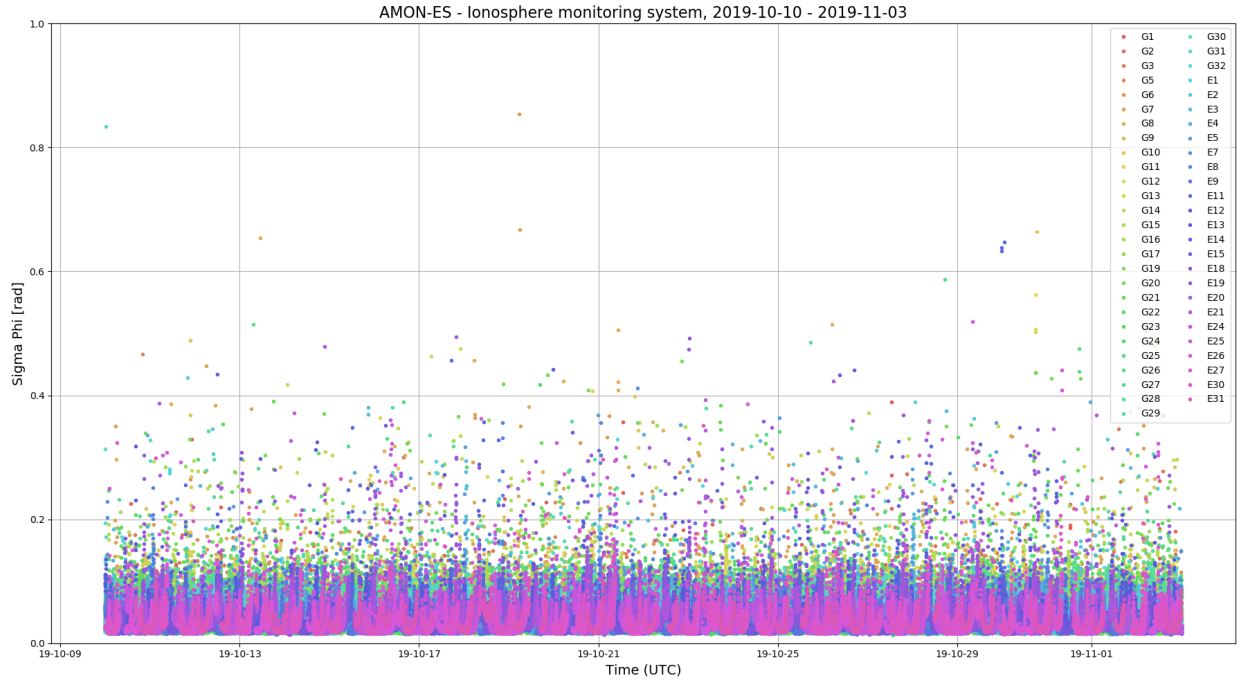


Figure 3.12: The series of σ_ϕ index measured during 10 October - 3 November 2019. The color coding is according to the specific GPS and Galileo satellites. The time resolution is 1 minute.

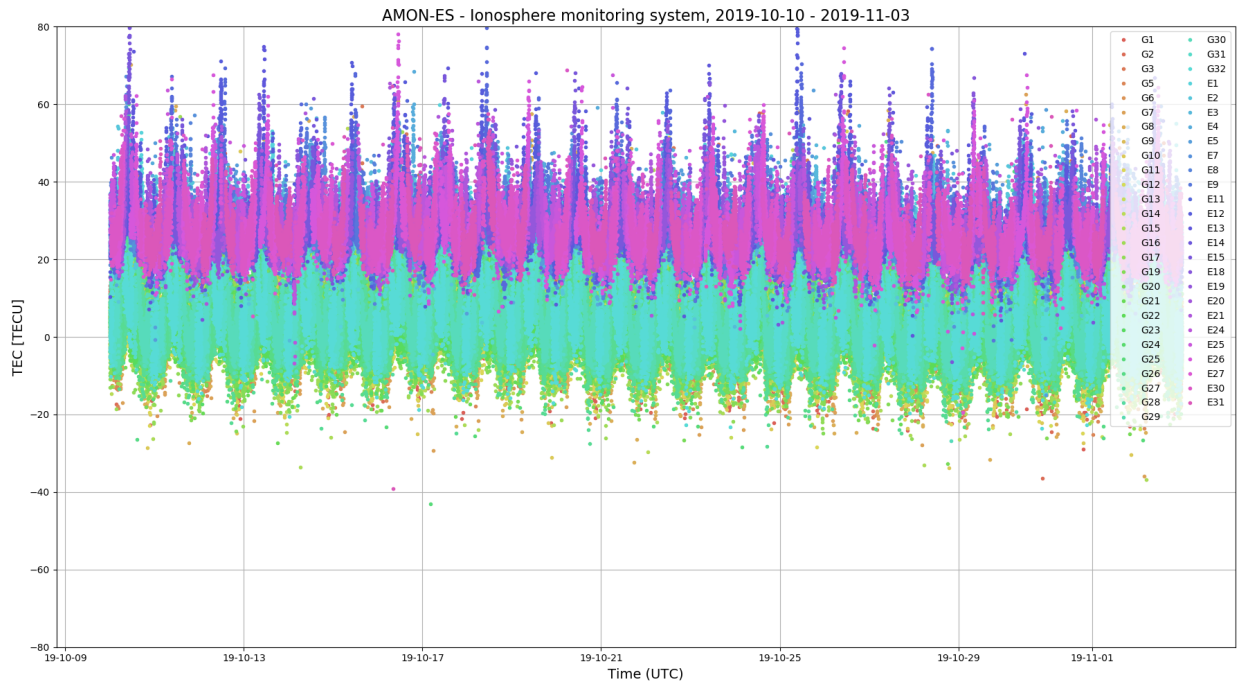


Figure 3.13: The series of TEC measured during 10 October - 3 November 2019. The color coding is according to the specific GPS and Galileo satellites. The time resolution is 1 minute.

In the "Feasibility study to observe ionospheric disturbances by one pixel UV detector" (SK1-05) activity we have investigated the occurrence of the upper atmosphere disturbances caused mainly by geomagnetic storms. However, during the time-frame of SK2-09 activity the solar activity has been in its minimum as it was expected. There were only a few minor (G1) geomagnetic storms within last year. One of them was during the time frame presented in Figures 3.10 - 3.13. The basic space weather parameters as Kp index, Dst index and F10.7 index for the same time frame are plotted in Figure 3.14.

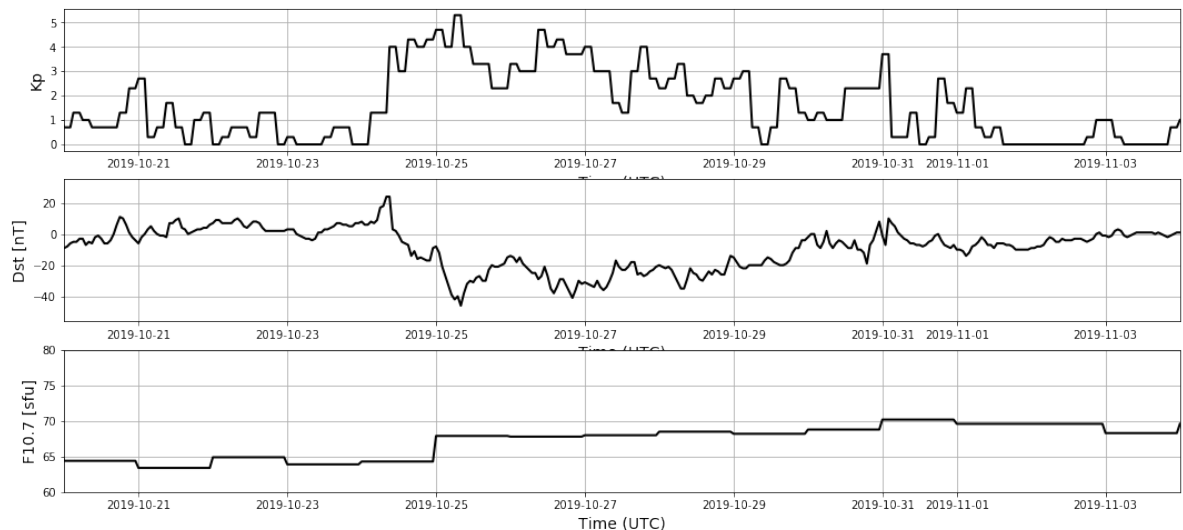


Figure 3.14: The series of Kp index (*top*), Dst index (*middle*), and F10.7 solar flux index (*bottom*) measured during 20 October - 3 November 2019.

The minor geomagnetic storm caused by solar particles released by coronal hole (CH75+) occurred on 24 - 25 October 2019. Its occurrence is represented by increase of K_p index and sharp decrease of Dst index. Both indexes are global and as it was concluded in the SK1-05 activity, their representation for the local environment (in upper atmosphere for specific latitude and longitude) might be not so straightforward. We have investigated if this geomagnetic storm was visible in local environment above AMON-ES. It is important to focus on the specific region on the sky by the observation from the ground. The Figures 3.10 - 3.13 contains data from the GNSS satellites distributed in all altitudes above horizon and with different azimuths. Therefore it is impossible to detect local characteristics in these complex images. For these reason we have selected only a specific region for the further investigation (Figure 3.15 (*right*)).

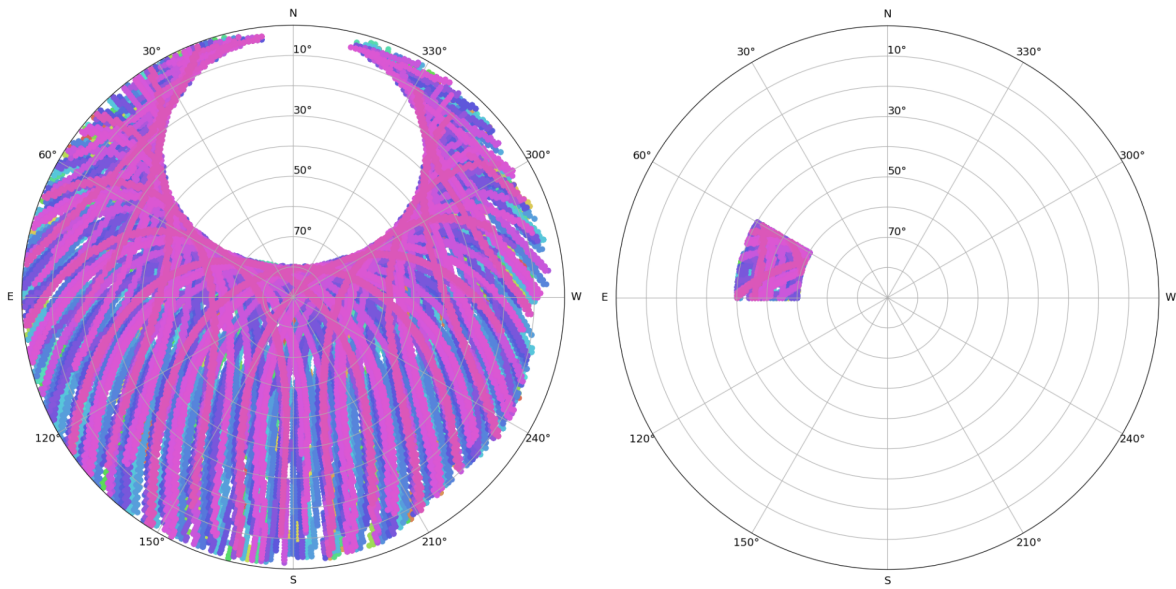


Figure 3.15: The positions of GNSS satellites (GPS and Galileo) on the sky by observation of AMON-ES. (*Left:*) The satellites' azimuth and elevation during the period 10 October - 3 November 2019. Based on these measurements the Figures 3.10 - 3.13 were produced. (*Right:*) The satellites' azimuth and elevation during the period 20 October - 1 November 2019 in the selected region - (azimuth: 60° - 90°, elevation: 40° - 60°). Based on these measurements the Figures 3.16 - 3.18 were produced.

The scintillation indexes S_4 and σ_ϕ for this specific sky region measured within 20 October - 1 November are displayed in Figures 3.16 and 3.17. The measured values represent the ionospheric conditions without ionospheric scintillations. However, the variation in the total electron content (TEC) can be detected in Figure 3.18. Such a diurnal variation is consistent with mid-latitude TEC variation during quiet helio-geomagnetic conditions described by e.g. [2]. In general it could be concluded that the minor geomagnetic storm that occurred on 24 - 25 October 2019 did not generate significant disturbances that could be easily recognised in the local ionospheric conditions.

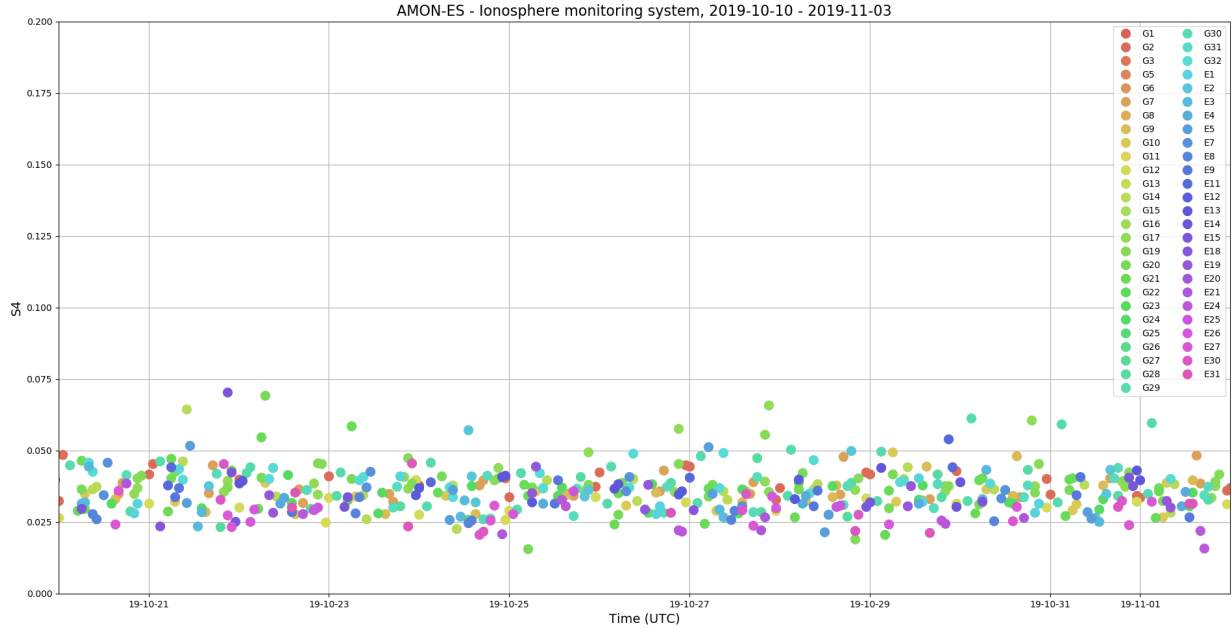


Figure 3.16: The series of S_4 index measured for the specific interval of satellites' azimuth and elevation (Figure 3.15 (right)) during 20 October - 1 November 2019. The color coding is according to the specific GPS and Galileo satellites. Each point represent 1 hour average.

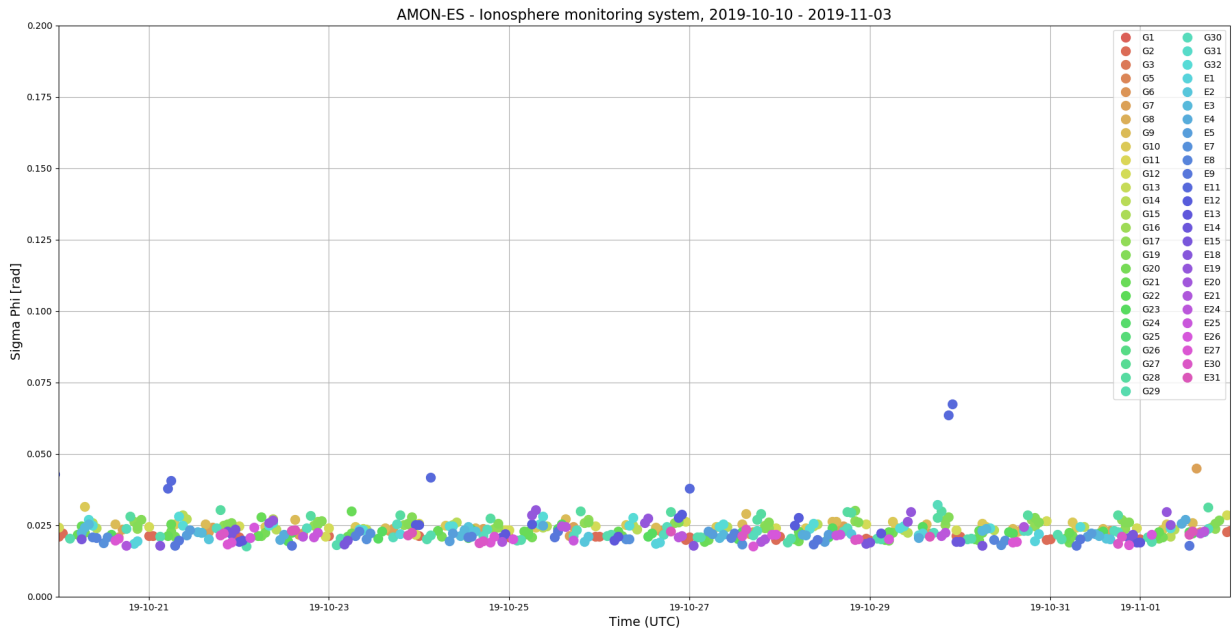


Figure 3.17: The series of σ_ϕ index measured for the specific interval of satellites' azimuth and elevation (Figure 3.15 (right)) during 20 October - 1 November 2019. The color coding is according to the specific GPS and Galileo satellites. Each point represent 1 hour average.

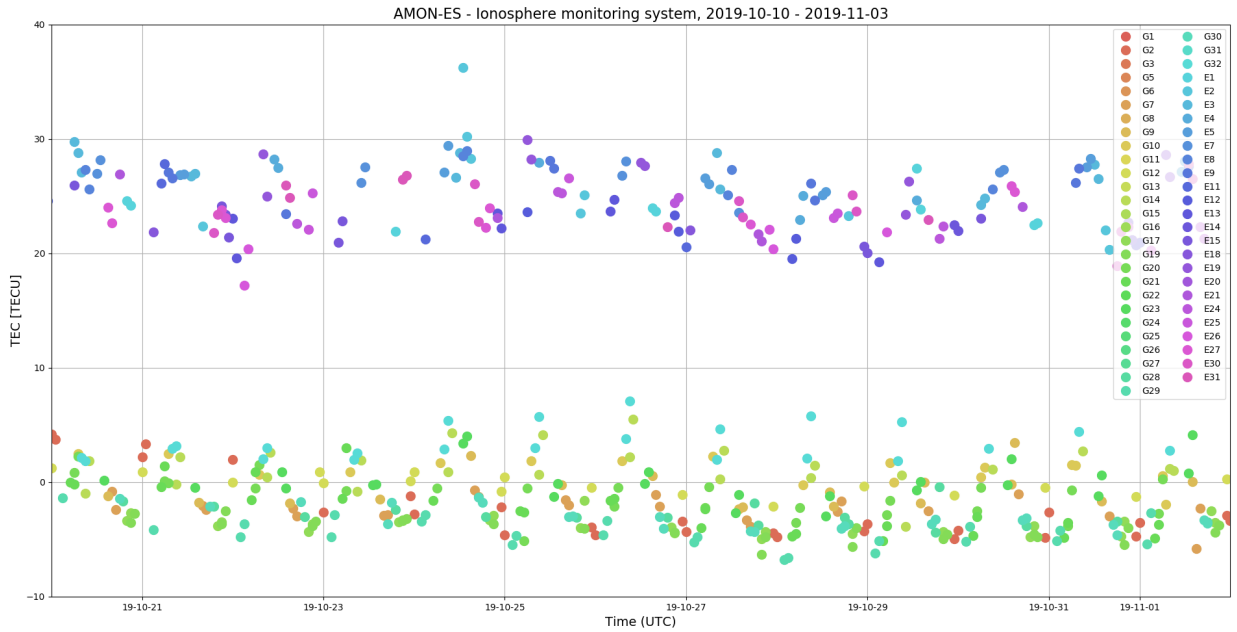


Figure 3.18: The series of TEC measured for the specific interval of satellites' azimuth and elevation (Figure 3.15 (*right*)) during 20 October - 1 November 2019. The color coding is according to the specific GPS and Galileo satellites. Each point represent 1 hour average.

The AMON measurements for the similar time interval as it is in Figure 3.18 is displayed in Figure 3.19. For the better visualization these same measurements are stacked together in Figure 3.20 to omit the daytime. The total length of measurements is ≈ 72 hours within 12 nights. The airglow intensity varies in interval $\pm 25\%$ of the average value. This is the evidence that AMON instrument is able to detect high dynamic environment of thermosphere. But the open question is, what is the source and mechanism of these dynamics? And also what is the connection of these variations of thermosphere to disturbances in ionosphere?

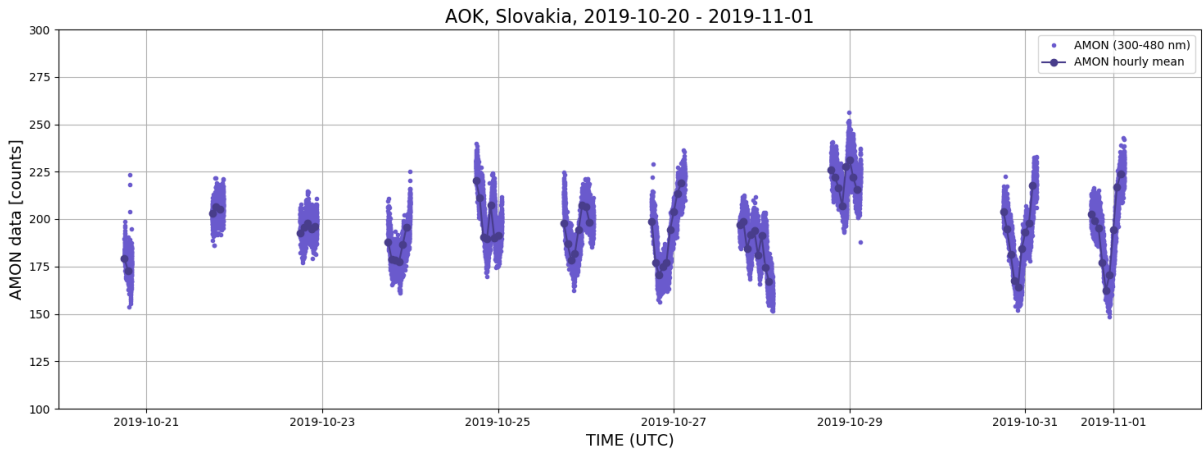


Figure 3.19: The series of airglow measurements by AMON during moonless and cloudless nights within time interval 20 October - 1 November 2019.

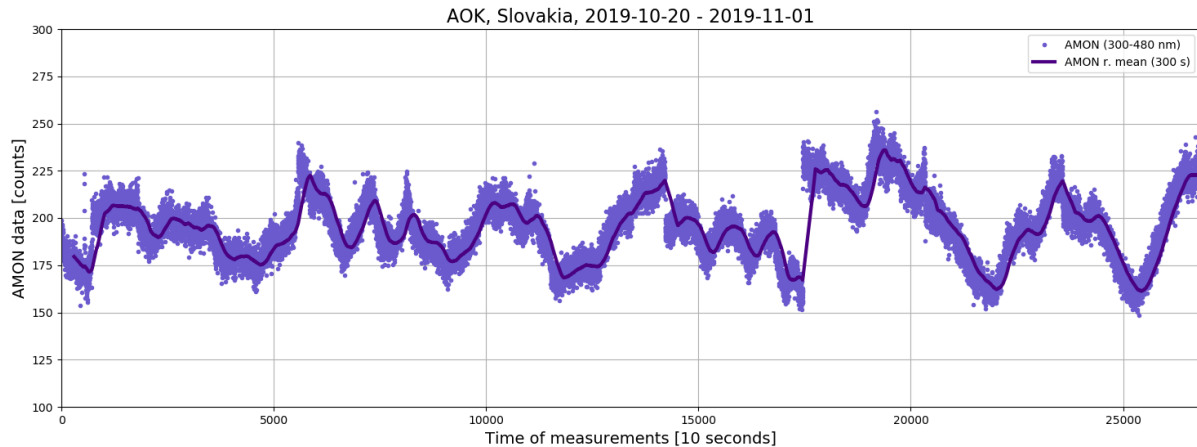


Figure 3.20: The same as in Figure 3.19 but the daytime intervals are omitted. The measurements are stacked together for better visualization purposes.

The answers are not straightforward but further studies will be performed. Multi spectral and multi instrumental measurements might be very beneficial in this effort as they could provide more complex monitoring of current situation. The example of such multi-messenger monitoring is displayed in Figure 3.21. The measurements of airglow radiation by AMON and AAC instruments are presented together with the measurements of TEC in ionosphere that is based on radio communication with GPS satellites. The consistency of measurements of UV airglow and green airglow (row 1 and row 2) was expected as it is discussed in Section 3.1. Interesting is the enhancement of UV and green airglow radiation during the time 21:00 - 23:30 (UTC). During this time the overall atmospheric conditions were stable as it is controlled by images in N filter (row 3). On the other hand the IR airglow intensity observed in I filter was significantly reduced during this time. This phenomenon of anti-correlation of airglow measurements in green and IR filters was reported also in TN-TS (Figure 4.6). The red airglow radiation (row 4) was stable during the night that is consistent with the stable values of TEC (row 6). The connection between red airglow and TEC is also discussed in TN-TS and e.g. in [3]. This Figure 3.21 demonstrate that AMON can detect the variations in the thermosphere by airglow measurements. These variations are probably not connected to geomagnetic activity even the minor geomagnetic storm was developed in the same time. The thermosphere-ionosphere system is very complex and therefore the presented multi-messenger approach is needed for as precise description as possible.

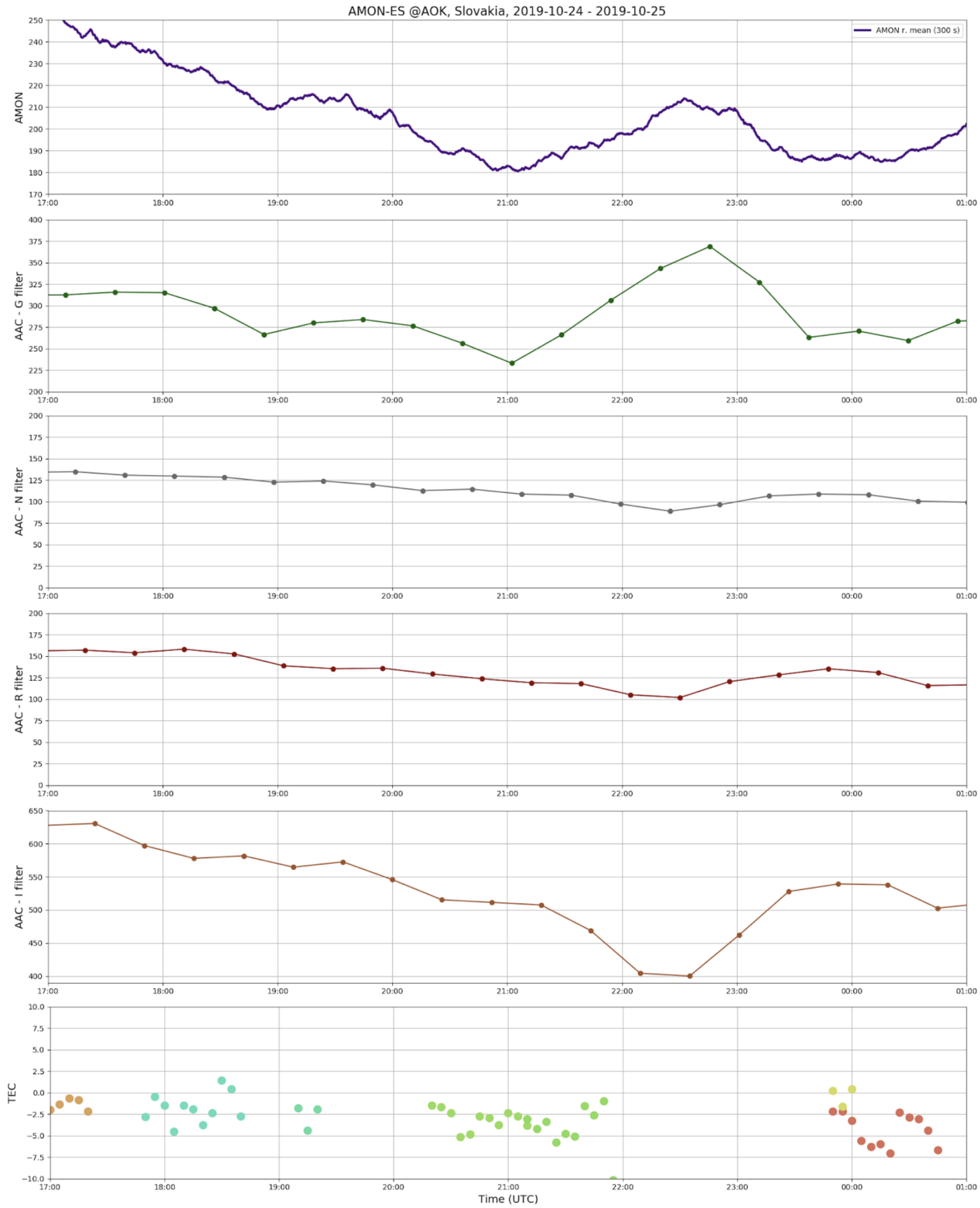


Figure 3.21: The series of airglow measurements during the night 24 - 25 October 2019 by AMON instrument (row 1), by AAC instrument in 4 filters (see Figure 3.3) (rows 2–5), and measurements of TEC by AMON-ES GNSS receiver evaluated from GPS radio signal (row 6). The points in rows 2–5 are the averaged values of pixels within interval 750–950 for x direction and 1400–1600 for y direction. Example of images in 4 filters in one time is in Figure 3.22.

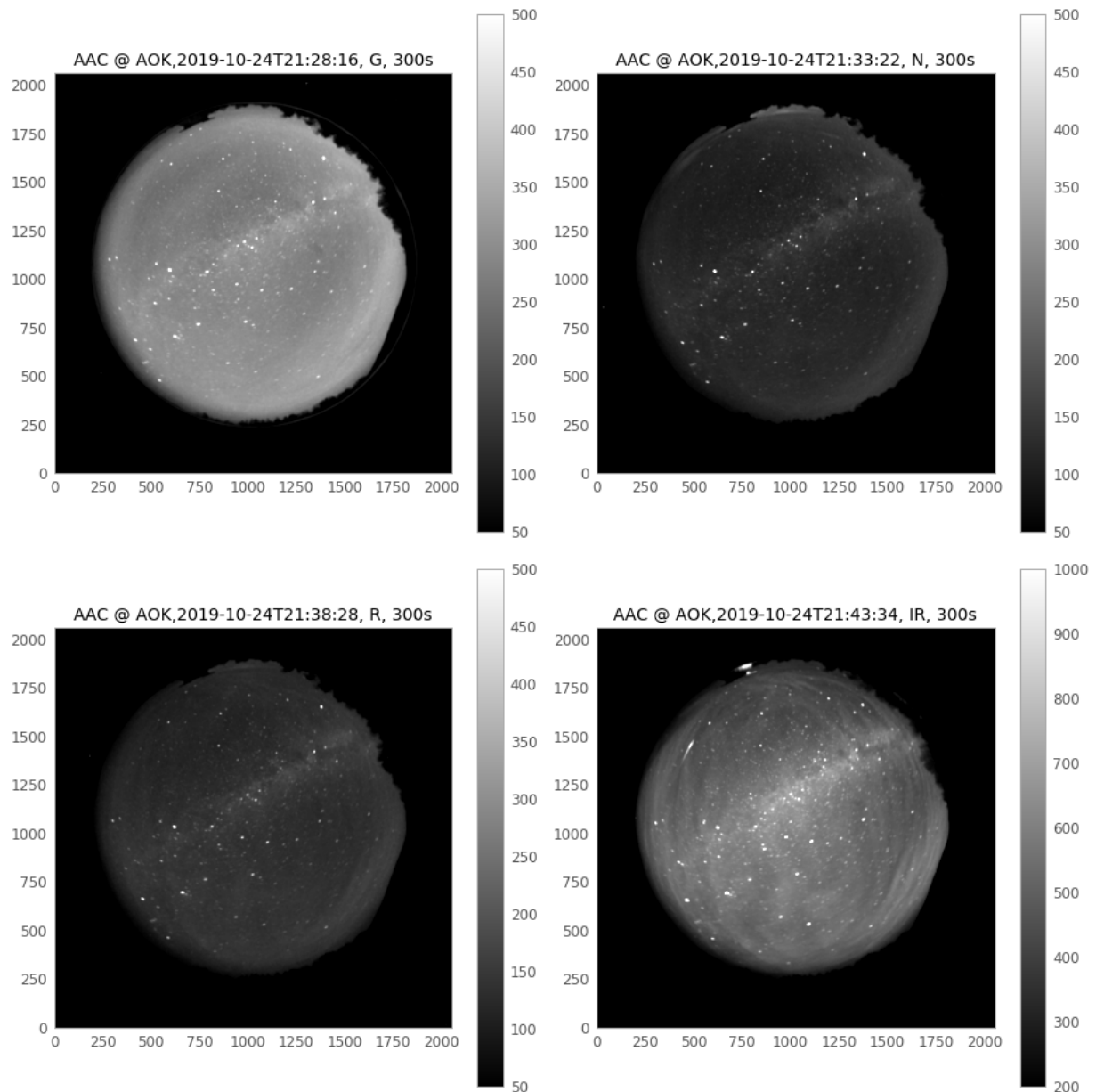


Figure 3.22: The example of images in 4 filters that were used for calculation of averaged intensity for Figure 3.21 - rows 2–5. The airglow variability is visible at a glance.

3.3 Weather monitoring system

The one of the basic requirement for AMON-ES was SRS-1011: The cloud monitor sensor that will recognize clear sky conditions shall be employed in the AMON-ES (see TN-SRS for more details). The components for weather monitoring systems were assembled in the the DSP laboratory in August and they were installed at AOK in September 2019. Since than the system is operating continuously during day and night. The weather monitor system consists of Raspberry-Pi camera with resolution 2592×1944 pixels that is operated by Raspberri-Pi computer. The images of the sky above AOK are automatically acquired each 10 minutes and consequently stored to the main computer - AMON-ES operation server. The examples of the images during cloudy conditions and during clear sky conditions are displayed in Figure 3.23 and Figure 3.24, respectively. The disadvantage of this camera is its low sensitivity during the night when the airglow observations are conducted. Therefore the second instrument for the cloud detection is employed. It is an infrared sensor with the wavelength range $10 - 11.5 \mu\text{m}$ that is able to measure the sky temperature. The sensor is integrated within the AAG CloudWatcher cloud detector (see MAITP-AE for more details). The example of the measurements for the time period 30 - 31 October 2019 is displayed in Figure 3.25. The low sky temperatures without rapid changes represent the clear sky conditions. It is evident that the conditions for the night 30 - 31 October were suitable for observation of airglow presented in Figure 3.9. During the analysis of the airglow measurements the weather conditions are controlled by using the stored weather monitor data.

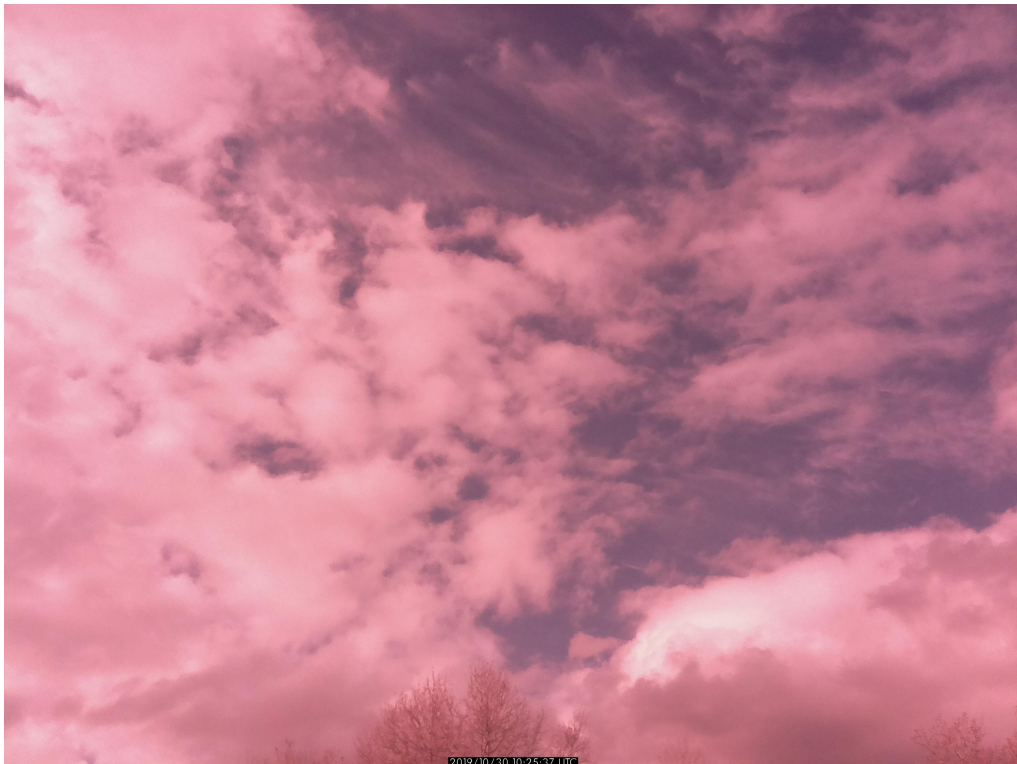


Figure 3.23: The image of sky above the Astronomical Observatory on Kolonica Saddle (AOK) on 30 October 2019 at 10:25. The low clouds and high clouds can be recognised.

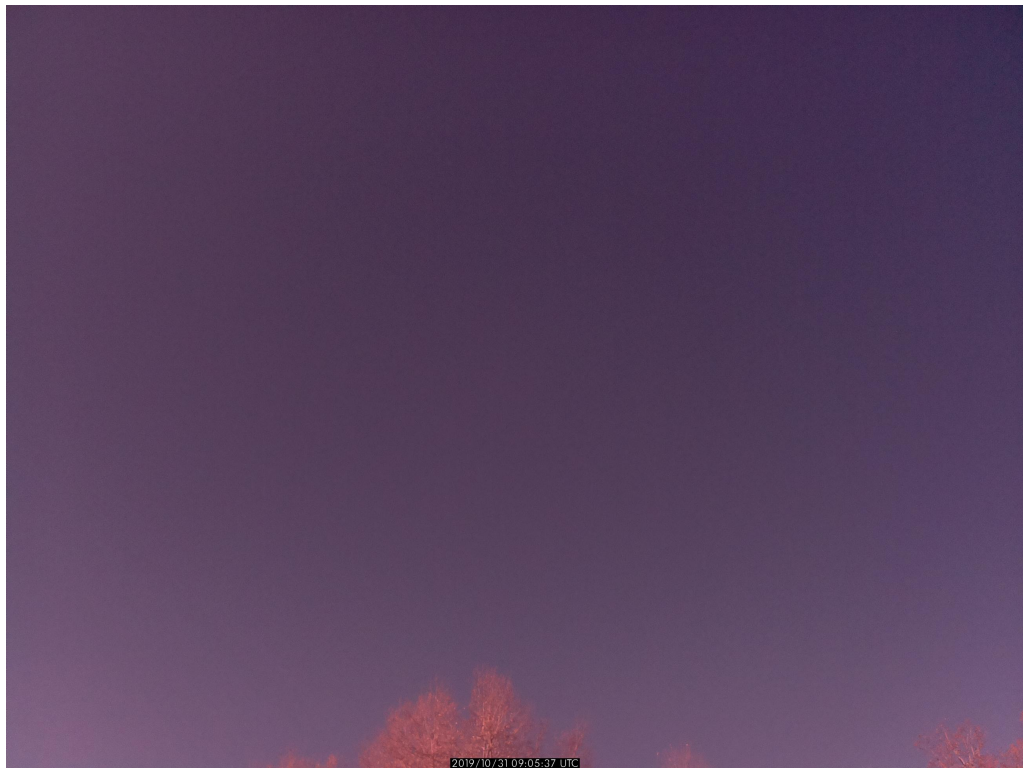


Figure 3.24: The image of sky above the AOK on 31 October 2019 at 09:05. The clear sky conditions are evident.

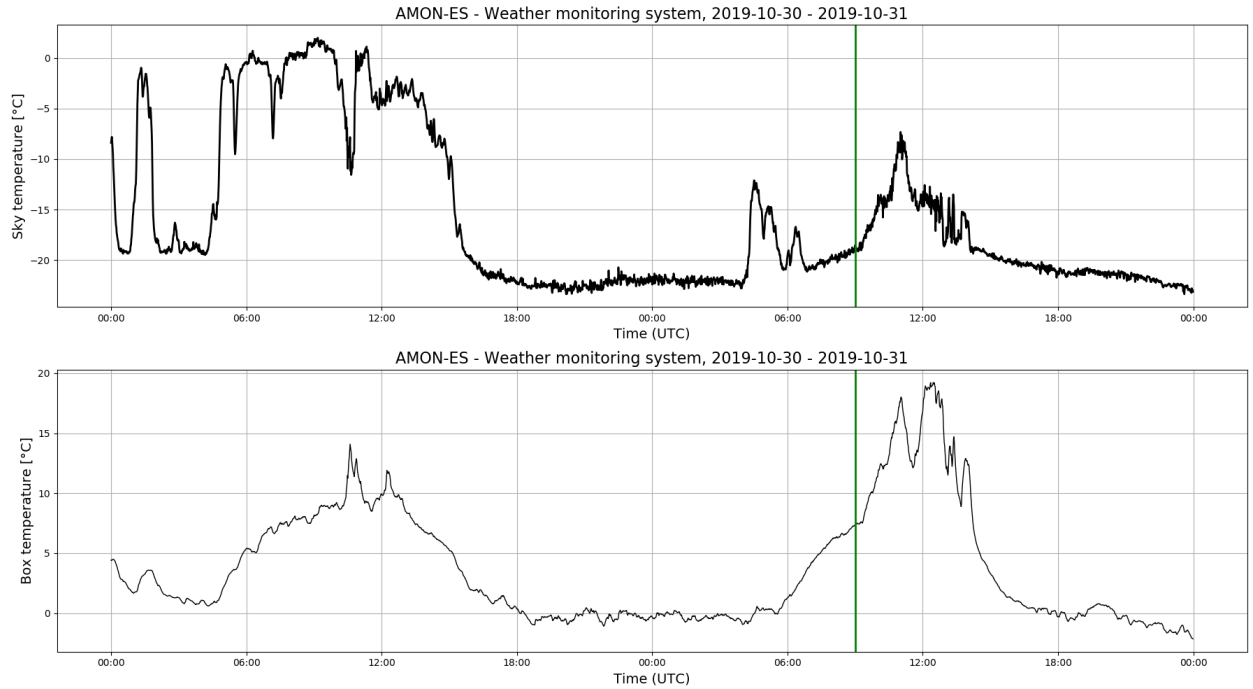


Figure 3.25: The sky (*top*) and detector (*bottom*) temperatures measured by AAG Cloud-Watcher during the time period 30 - 31 October 2019. The time of clear sky situation presented in Figure 3.24 is marked by green vertical line.

Chapter 4

Conclusions and Next steps

The Airglow MONitor - Extended Station (AMON-ES) was constructed on Astronomical Observatory on Kolonica Saddle (AOK) in the spring 2019. It is in the operation since May 2019. The weather and astronomical conditions (cloudless and moonless nights) in October 2019 allowed almost continuous observations by AMON-ES within 12 consecutive nights. The data were acquired from 3 AMON-ES subsystems - airglow monitoring system, ionosphere monitoring system and weather monitoring system. Based on these data the following findings were obtained:

- AMON-ES is a unique station within Slovakia for monitoring of thermosphere-ionosphere system.
- AMON-ES is fully operational and all requirements from TN-SRS and MAITP-AE were fulfilled.
- Thanks to weather monitor system, the cloudless nights can be effectively selected for further analyses.
- The AMON All-sky Camera (AAC) has capability to provide high-resolution all-sky images of green airglow (OI 557.7 nm), red airglow (OI 630.0 nm) and infrared airglow (OH 700–900 nm). The airglow variation and its development through the night caused by e.g. AGW can be recognised at a glance.
- The astronomical background can be effectively subtracted from the AAC airglow images by image in N filter.
- The AMON measurements of UV airglow (300-480 nm) are in very good agreement with the measurements of green airglow by AAC in G filter. This is the evidence that the AMON design and capabilities are suitable for airglow monitoring even if its constructions costs are roughly 10 times smaller than the costs of AAC. (It is noted that the costs of AAC are roughly 10 times smaller than the costs of standard airglow imagers).
- The AMON does not provide spatial resolution of airglow structures in particular time but it provides very high temporal resolution. So it is capable to detect all variations in the lower thermosphere that pass through its field of view.

- Thanks to combination of AMON and AAC data, the airglow science can be performed and the processes in the thermosphere can be studied.
- The ionospheric monitoring system is in operation on AMON-ES. It provides continuous and reliable data of ionospheric indexes S_4 , σ_ϕ , SI and TEC. The positions of GPS and Galileo satellites can be also tracked.
- The connection between minor geomagnetic storms and local variations of ionosphere might be not straightforward. The AMON-ES ionosphere monitoring system did not detect significant changes in measured parameter caused by minor geomagnetic storm that occurred during night 24 - 25 October 2019. These connections need will be studied in the future during the years of next maximum of solar cycle.
- The source of the disturbances in thermosphere-ionosphere system might be caused by different phenomena. Therefore the multi-messenger approach of observation might be beneficial for uncovering these processes.

The routine operation of AMON-ES will continue through the year 2020. It is planned to publish the obtained results in the scientific paper. But the main goal of the results listed above was to obtain better understanding what are the AMON instrument's detection capabilities. Based on this knowledge, the AMON instrument will be improved and configured. The new version a.k.a. AMON3 will be then tested and calibrated in the laboratory conditions and then used as a main part for AMON-net.